Science of Sintering, **51** (2019) 389-399

doi:https://doi.org/10.2298/SOS1904389S

UDK: 532.74; 53.086; 661.112.3; 666.3.019

Structure and Microstructure Characterization of the $La_2SrB_{10}O_{19}$ Glass-ceramics

Jovica N. Stojanović[1*)], Sonja V. Smiljanić[2], Snežana R. Grujić[2], Predrag J. Vulić[3], Srđan D. Matijašević[1], Jelena D. Nikolić[1], Veljko Savić[1]

[1]Institute for Technology of Nuclear and Other Mineral Raw Materials, Franchet d'Esperey 86, PO Box 390, 11000 Belgrade, Serbia

[2]Faculty of Technology and Metallurgy, University of Belgrade, Karnegijeva 4, 11000 Belgrade, Serbia

[3]Faculty of Mining and Geology, University of Belgrade, Đušina 7, 11000 Belgrade, Serbia

Abstract:

The crystal structure of new lanthanum strontium borate glass-ceramics was refined by the Rietveld method. The results showed that $La_2SrB_{10}O_{19}$ has the monoclinic crystal structure, space group C2 (No. 5) with a = 11.1170(6), b = 6.5667(3), c = 9.2363(3) Å, β = 91.481°, V = 674.04(7) Å^3, two formula units per unit-cell, and density 3.830 g cm^{-3}. The main building units of the crystal structure are BO_4 tetrahedra and BO_3 triangles. Clusters composed of $[B_5O_{12}]$ form an infinite double layer running perpendicular to the c-axis. Lanthanum atoms, situated in $[B_5O_{12}]_n$ layers, are coordinated with 10 oxygen atom in a form of LaO_{10} polyhedra, while Sr atoms, located between $[B_5O_{12}]_n$ layers, are coordinated with 8 oxygen atoms in a form of SrO_8 polyhedra. Microstructural measurements contain both crystallite domain sizes and microstrain calculations obtained by the Warren-Averbach and the simplified integral-breadth methods.

Keywords*: Glass-ceramics; Sintering; X-ray diffraction; Crystal structure and microstructure; Rietveld refinement.*

1. Introduction

In recent years, a lot of scientific efforts have been put in studying new non-linear optical materials (NLO) due to their application in electronic devices. Borate crystals are used as solid-state laser hosts and as NLO materials with good second harmonic generation (SHG) efficiency [1].

Lanthanide borate glasses and glass-ceramics are recognized as materials for the application as laser hosts, NLO and in the optoelecrtonics [2]. The addition of lanthanum oxide in the alkaline earth borate glasses improves optical properties and chemical durability [3]. Wu *et al*. (2001) [4] identified the monoclinic phase $La_2CaB_{10}O_{19}$ (LCB) in the La_2O_3-CaO-B_2O_3 system. Cao *et al*. (2000) [5] published a paper describing the acquisition and characteristics of the crystalline phase $La_2SrB_{10}O_{19}$, expecting that this crystal display its good properties as NLO material as well as other advantages such as hardness and chemical resistance. The crystalline phase $La_2SrB_{10}O_{19}$ in that study was obtained by a classical solid-

*) **Corresponding author:** j.stojanovic@itnms.ac.rs

state reaction at elevated temperature. It has been shown that $La_2SrB_9O_{19}$ has the same structure as LCB.

In this paper, the crystalline phase $La_2SrB_{10}O_{19}$ is obtained through the process of glass crystallization. The aim of this paper is to review its structure and microstructure characteristics and to compare it with the literature data.

2. Materials and Experimental Procedures

The glass-ceramics sample with the following composition (mol %): La_2O_3, SrO, B_2O_3, 14.3, 14.3, 71.4, respectively were obtained by the sintering procedure. Reagent-grade H_3BO_3, $SrCO_3$ and $La_2(CO_3)_3$ were mixed and homogenized. All chemicals used were of reagent grade quality. The mixture was placed in a platinum crucible in an electric furnace and sintered at 1200 °C for 30 min. The platinum crucible was covered in order to minimize boron evaporation. The melt was cast and cooled on a stainless steel plate in air at room temperature. Measurements of the weight loss indicate that the samples are within 1–2 wt% of desired compositions. The obtained glass-ceramics sample was transparent, without visible bubbles [6-8].

The crystallization behavior of the glass-ceramics was investigated by DTA (SDT Q600 TGA/DS, TA Instruments, USA) with Al_2O_3 as the referent material. Powder (<0.048 mm) sample of about 10 mg was heated up to the melting point and cooled at 20 ^oC/min in a dry air atmosphere (flow rate 100 cm^3 min^{-1}).

The crystallization of bulk glass-ceramics samples was performed by heating the samples in a Carbolite CWF 13/13 electric furnace with automatic regulation and temperature accuracy of ± 1 °C up to 760 °C for 70 h. After the heat treatment, the samples were removed from the furnace, crushed and subjected to the XRPD analysis.

The X-ray diffraction pattern was collected using X-Ray powder diffractometer Rigaku SmartLab in Bragg-Brentano parafocusing geometry (CBO optics with BB slit), using ceramic Copper X-Ray tube with long fine focus (LFF) as radiation source. The voltage was 40 kV and current 30 mA. The Rietveld refinement data were collected by D/teX Ultra 250 strip detector in 8 – 135° 2θ angular range, with step of 0.01° and collection speed of 0.5 min/° 2θ. The crystal structure refinement of the glass-ceramics sample was obtained by the full structure matching mode of the Rietveld refinement technique [9], using the FULLPROF software [10]. The data for calculation of initial unit-cell parameters were collected from 5 – 70° 2θ angular range and calculated using the LSUCRIPC (least square unit cell refinement) software [11]. BREADTH software was used for the diffraction-line broadening measurements [12]. Drawings of structural details were produced using the ATOMS software [13]. Bond valence sum calculations were obtained using VALIST software [14].

The pycnometer method (V = 5 ml^3; in liquid xyilol) was used for density measurements.

3. Results and Discussion

3.1. DTA and XRPD analysis

The characteristic temperatures were determined from the DTA result. The small endothermic shoulder on the DTA curve represents the glass transition temperature at T_g, 650 °C, the temperature, T_x, crystallization onset, was determined by extrapolation at 750 °C. The exothermic temperature peak T_p (780 °C) at the DTA curve corresponds to the crystallization of glass, and the endothermic peak corresponds to the melting of the glass at 947 °C. According to the DTA it can be concluded that crystallization did not take place during the

cooling process of the sample (Fig. 1a). XRPD results showed that the polymorphic crystallization occurred in this glass-ceramics and the $La_2SrB_{10}O_{19}$ phase was formed (Fig. 1b). The initial unit-cell parameters are in excellent agreement with the only literature data for $La_2SrB_{10}O_{19}$ [4], and expectedly higher than data for isostructural $La_2CaB_{10}O_{19}$ published by Cao *et al.* (2000) [5, 6]. DTA curve of the glass and XRPD of the crystallized glass-ceramics sample are shown in Fig. 1.

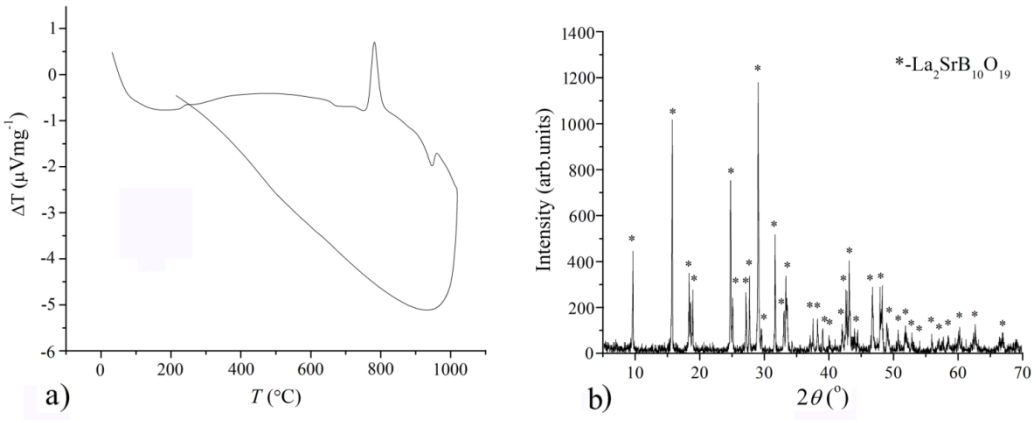

Fig. 1. a) DTA curve of the glass and b) XRPD of the crystallized glass-ceramics sample.

3.2. Crystal structure refinement by the Rietveld method

Atomic coordinates of $La_2CaB_{10}O_{19}$ compound were used as initial for crystal structure refinement [4]. A total of 176 parameters were varied during the refinement process: a scale factor, 100 background parameters, three profile, one asymmetry and two profile mixing parameters. In addition to these, non-structural parameters, the unit-cell parameters, 46 positional parameters of all atoms, and 17 isotropic displacement parameters of each atomic site were varied. The maximal ratio of the parameter shift to their standard deviation was $\Delta/\sigma<0.1$. The background was refined as linear interpolation between a set background points with refinable heights. A pseudo-Voigt profile shape function was used to model the diffraction profiles parameters. The experimental conditions and crystallographic data are listed in Table I. The fractional atomic coordinates with isotropic or equivalent isotropic displacement parameters for $La_2SrB_{10}O_{19}$ are presented in Table II. The Rietveld refinement plot of $La_2SrB_{10}O_{19}$ is shown in Fig. 2.

Tab. I The experimental conditions and crystallographic data for $La_2SrB_{10}O_{19}$.

Sample characterization			
Name (chemical, mineral)	Dilanthanum Strontium Decaborate		
Empirical formula	$La_2SrB_{10}O_{19}$		
Source/preparation	Synthetic		
Powder data collection			
Radiation type, source	X-rays, Cu λ value used	1.54060Å $K\alpha_1$/1.54439 $K\alpha_2$	
Monochromator	diffracted beam	graphite monochromator	
Detector (film, scint. etc)	proportional		
Instrument description (type, slits)	vertical diffractometer divergence slit 1° receiving slit 0.1 mm soller slit 1°		
Instrumental profile breadth	0.10 °2θ	temp. (°C)	25 ± 1

Specimen form/particle size	edge loaded powder/ <10 μm particle size
Profile range ($^o2\theta$)	from 8 to 135
Step width ($^o2\theta$)	0.01
Collection speed	0.5 min/° 2θ
Number of observations	2750
Asymmetry correction ($^o2\theta$)	30.0
Specimen motion	horizontal
Crystal parameters	
Unit-cell parameters	a=11.1170(6), b=6.5667(3), c=9.2363(3) Å,
V (Å^3)	β=91.481(3) ^{o}
Z	674.04(7)
D_x (g/cm^3)	2
D_m (g/cm^3)	3.830
	3.878
Formula wt.	777.52 g/mol
Crystal system	monoclinic
Space group	$C2$ (5)
	least square unit-cell refinement method
Reliability factors	
R_p ($100\cdot\Sigma\|y_{io}-y_{ic}\|/\Sigma\|y_{io}\|$)	12.7
R_{wp} ($100\cdot[\Sigma w_i(y_{io}-y_{ic})^2/\Sigma w_i\cdot y_{io}^2]^{½}$)	17.7
R_{exp} ($100\cdot[N\text{-}P/\Sigma w_i\cdot y_{io}^2]^{½}$)	8.09
R_B ($100\cdot\Sigma\|I_o-I_c\|/\Sigma\|I_o\|$)	14.4
R_F ($100\cdot\Sigma\|F_o-F_c\|/\Sigma\|F_o\|$))	3.86
Gof-index	1.7

Tab. II Fractional atomic coordinates and isotropic or equivalent isotropic displacement parameters for $La_2SrB_{10}O_{19}$.

atom	x	y	z	U_{iso}/U_{eq} (A^2)
La	0.16600(18)	0	0.14020(20)	0.0090(3)
Sr	0	0.8170(2)	1/2	0.0121(3)
O1	0	0.7761(4)	0	0.015(1)
O2	0.39230(13)	0.9928(2)	0.1578(5)	0.013(1)
O3	0.32860(12)	0.3139(4)	0.1534(6)	0.016(1)
O4	0.9442(3)	0.1173(3)	0.1481(5)	0.017(1)
O5	0.21817(14)	0.6292(6)	0.1742(4)	0.013(1)
O6	0.07422(11)	0.3783(4)	0.1988(5)	0.015(1)
O7	0.05252(10)	0.74510(19)	0.22051(10)	0.013(1)
O8	0.1965(4)	0.9576(7)	0.4117(3)	0.019(1)
O9	0.85295(13)	0.5456(10)	0.56886(14)	0.019(1)
O10	0.14630(11)	0.987(2)	0.63724(8)	0.014(1)
B1	0.44066(7)	0.20261(14)	0.13231(10)	0.017(1)
B2	0.95658(9)	0.31904(12)	0.1853(3)	0.020(1)
B3	0.33084(7)	0.52289(13)	0.21005(9)	0.023(1)
B4	0.12144(9)	0.56618(13)	0.27169(8)	0.026(1)
B5	0.23225(7)	0.0686(3)	0.52714(11)	0.029(1)

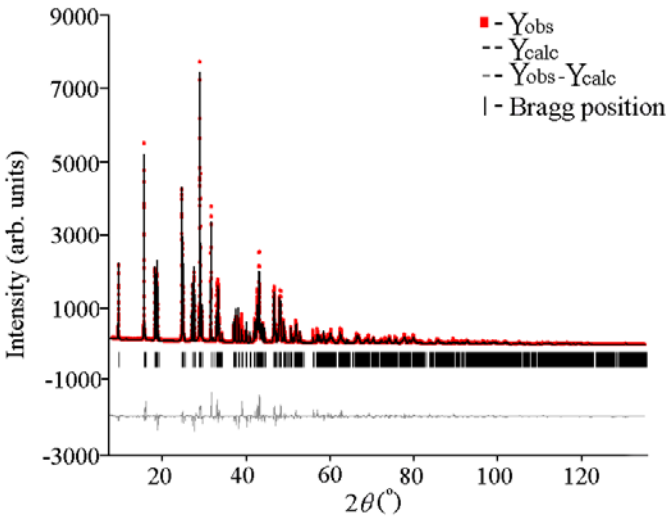

Fig. 2. The Rietveld refinement plot of $La_2SrB_{10}O_{19}$.

The main building units of the crystal structure consist of BO_4 tetrahedra and BO_3 triangles in a form of $[B_5O_{12}]$ clusters. The $[B_5O_{12}]$ consists of three BO_4 tetrahedra, and two BO_3 triangles connected *via* oxygen atoms (Fig. 3). These units are mutually interconnected *via* O3 and O4 into infinite $[B_5O_{12}]_n$ layers perpendicular to the *c*-axis. Furthermore, these layers are bonded to O1 thus forming a double layer (Fig. 5).

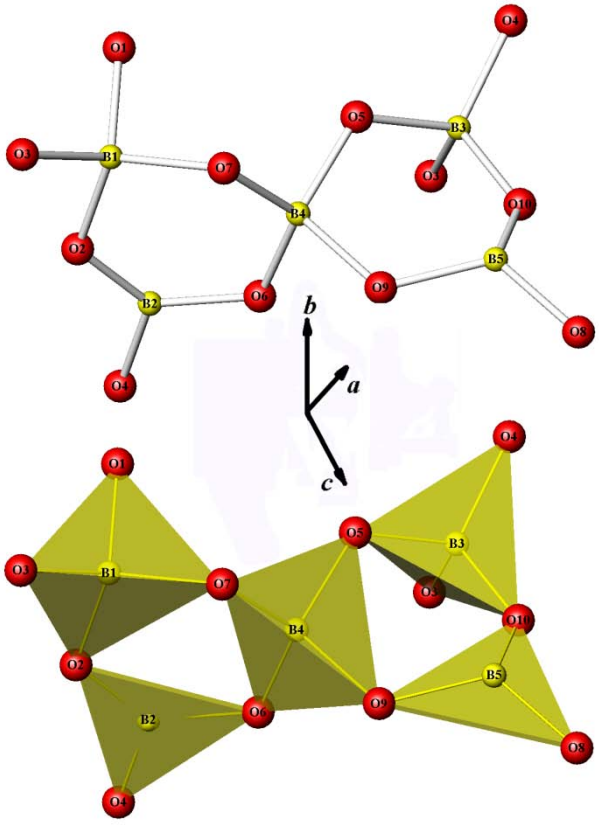

Fig. 3. The $[B_5O_{12}]$ building unit.

Lanthanum atoms, situated in $[B_5O_{12}]_n$ layers, are coordinated with 10 oxygen atom in a form of LaO_{10} polyhedra. These polyhedra are linked to one another through face-sharing O4 and O1, and vertex-sharing O3 oxygen atoms thus forming infinite layers also perpendicular to the *c*-axis. Sr atoms, located between $[B_5O_{12}]_n$ layers, are coordinated with 8 oxygen atoms. SrO_8 and LaO_{10} polyhedra are bonded to each other by edge-sharing O7 and O8 oxygen atoms (Fig. 4). The polyhedral presentation of the $La_2SrB_{10}O_{19}$ crystal structure is presented in Fig. 5.

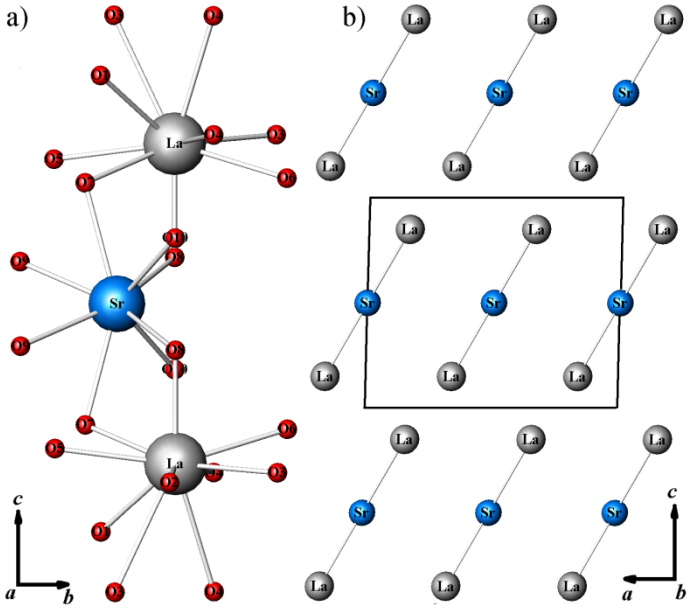

Fig. 4. a) the LaO_{10}–SrO_8–LaO_{10} trimer, b) [*h* 0 *h*/2] orientation of La–Sr–La cations with the unit-cell outlined.

Average bong lengths in the polyhedra are as follows: <LaO_{10}> = 2.655 Å, <SrO_8> = 2.593 Å, <$B1O_4$> = 1.486 Å, <$B2O_3$> = 1.371 Å, <$B3O_4$> = 1.481 Å, <$B4O_4$> = 1.485 Å, <$B5O_3$> = 1.385 Å. The calculated average bond distances are in very good agreement with the literature data [4] except for Ca–O, which has expectedly lower value (<CaO_8> = 2.465 Å). Selected bond lengths for $La_2SrB_{10}O_{19}$ are given in Table III.

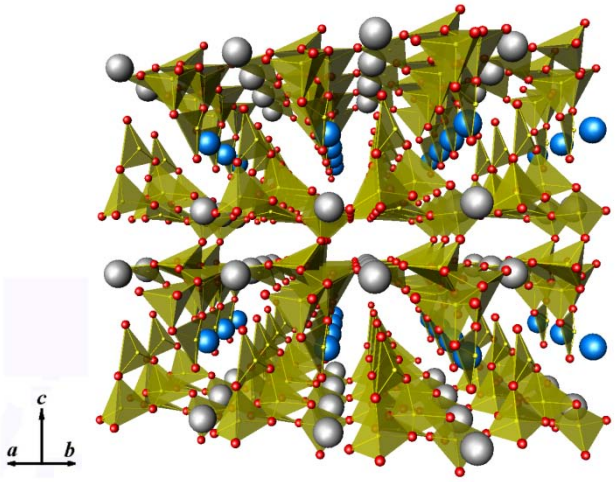

Fig. 5. A perspective polyhedral presentation of the $La_2SrB_{10}O_{19}$ crystal structure. Yellow-BO_4 tetrahedra and BO_3 triangles, gray spheres-La atoms, blue spheres-Sr atoms.

Tab. III Selected bond lengths for $La_2SrB_{10}O_{19}$.

bond	length (Å)	bond	length (Å)
La–O7	2.236(2)	B1–O3	1.462(2)
La–O2	2.518(2)	B1–O1^{iv}	1.4853(12)
La–O5	2.523(4)	B1–O7^{iv}	1.4962(13)
La–O8	2.540(3)	B1–O2	1.5012(17)
La–O4	2.587(4)	B2–O6	1.3676(17)
La–O1	2.671(2)	B2–O2^{v}	1.3679(18)
La–O3	2.744(3)	B2–O4	1.376(2)
La–O6	2.747(3)	B3–O10^{vi}	1.4608(12)
La–O3^{ii}	2.979(5)	B3–O5	1.465(3)
La–O4^{i}	3.006(5)	B3–O3^{vii}	1.470(3)
Sr–O9	2.513(5)	B3–O4^{viii}	1.529(4)
Sr–O9^{iii}	2.513(5)	B4–O5	1.465(3)
Sr–O8	2.527(4)	B4–O7	1.4752(15)
Sr–O8^{iii}	2.527(4)	B4–O6^{vii}	1.496(3)
Sr–O10	2.6285(17)	B4–O9^{iii}	1.5003(16)
Sr–O10^{iii}	2.6285(17)	B5–O8	1.345(4)
Sr–O7	2.7051(10)	B5–O9^{iv}	1.3953(18)
Sr–O7^{iii}	2.7051(10)	B5–O10	1.4139(14)

Symmetry codes: (*i*) *–x, y, –z*; (*ii*) *–x+½, y–½, –z*;
(*iii*) *–x, y, –z+1*; (*iv*) *x+½, y+½, z*; (*v*) *x–½, y+½, z*;
(*vi*) *–x+½, y–½, –z+1*; (*vii*) *x, y–1, z*; (*viii*) *x+½, y–½, z*

3.3. Bond valence calculations (BVC)

The BVC of lanthanum and strontium showed that these atoms are oversaturated (3.22 and 2.26 v.u., respectively), indicating that these sites are slightly over bonded, due to short La–O7, Sr–O8 and Sr–O9 bond lengths. These values are in good agreement with lanthanum and calcium atoms (3.08 and 2.20 v.u., respectively) from literature data [4]. However, BVC values of boron are minimally undersaturated to ideal ranging from 2.90 for B5 to 3.00 v.u. for B2. Literature data are from almost ideal for B4 (2.99 v.u.) to somewhat oversaturated for B2 (3.07 v.u.) [4]. On the other hand, the bond valence sums for the oxygen atoms are from moderately undersaturated to slightly oversaturated, and range from 1.77 for O8 to 2.10 v.u. for O2, with the exception of O7 atom (2.49 v.u.). The significant oversaturation of O7 is due to the fact that it is connected to four atoms (La, Sr, B1, and B4) with one unusually short distance (La–O7). In addition, replacement of calcium with much larger strontium caused structure disorder, which is best manifested in bond lengths of LaO_{10} and SrO_8 polyhedra. Namely, oxygens with highest (O7) and lowest (O8) BVC values are bonded to both La and Sr atoms (Fig. 4a). In favor of this assumption are literature data [4] for oxygen atoms ranging from 1.92 for O5 to 2.14 v.u. for O2 (O7 and O8 amount to 2.08 and 1.97, respectively). BVC is shown in Table IV.

Tab. IV Results of bond valence sum Σv_{ij} (valence units) calculations for $La_2SrB_{10}O_{19}$.

	La	Sr	B1	B2	B3	B4	B5	Σv_{ij}
O1	0.260/0.520		0.734/1.468					1.99
O2	0.393		0.703	1.008				2.10
O3	0.213+0.113		0.782		0.765			1.87
O4	0.326+0.105			0.987	0.652			2.07
O5	0.387				0.776	0.776		1.94
O6	0.211			1.009		0.713		1.93
O7	0.841	0.205/0.410	0.713			0.755		2.49

O8	0.370	0.331/0.662					1.073	1.77
O9		0.344/0.688				0.705	0.936	1.99
O10		0.252/0.504			0.785		0.891	1.93
Σv_{ij}	3.22	2.26	2.93	3.00	2.98	2.95	2.90	

Factors (constants) R_o: La^{3+}–O^{2-} = 2.172 Å, Sr^{2+}–O^{2-} = 2.118 Å, B^{3+}–O^{2-} = 1.371 Å.

3.4. Crystallite size and microstrain measurements

Crystallite domain size and corresponding microstrain parameters were calculated by the Warren-Averbach (surface $<D>_s$- and volume $<D>_v$-weighted domain size, root-mean-square microstrain (RMSM) averaged over the $<D>_s$ and $<D>_v$ distances), and the simplified integral-breadth methods (volume-averaged domain size and upper limit of microstrain: Cauchy-Gauss function) [12]. It is widely accepted that the best approximation for a structural broadening of diffraction lines is a combination of the Cauchy and Gauss function i.e. the Voigt and pseudo-Voigt function. Cauchy component of crystallite domain size and Gaus component for microstrain of crystal lattice represents a very good theoretical basis and finds wide application in calculation of microstructural parameters of individual diffraction lines and in many software for the Rietveld analysis.

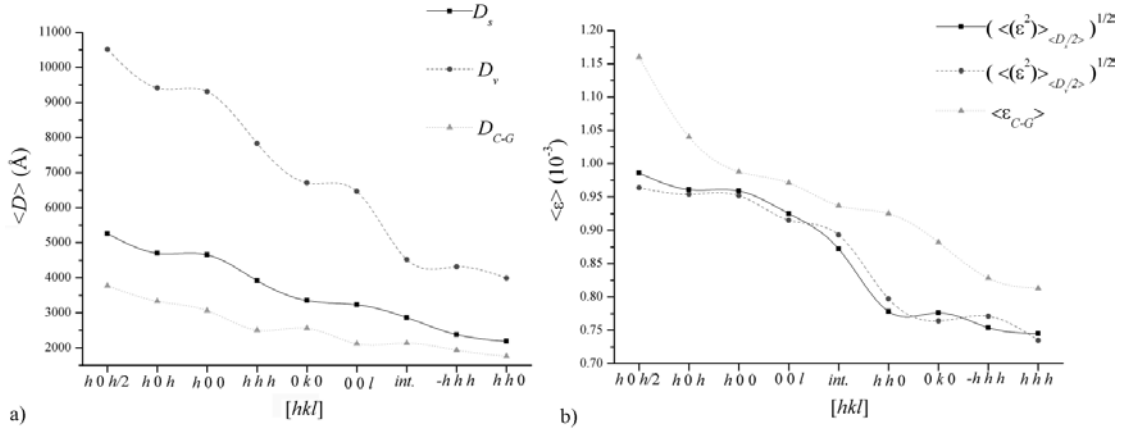

Fig. 6. a) crystallite domain size b) microstrain parameters graphic illustrations obtained by the Warren-Averbach and the simplified integral-breadth methods for $La_2SrB_{10}O_{19}$.

Microstructure calculations were obtained on 675 diffraction-line profiles (integral sample), and following crystallographic directions: [*h* 0 0] (2 0 0), (4 0 0), (6 0 0), (8 0 0), (10 0 0), (12 0 0); [0 *k* 0] (0 2 0), (0 4 0), (0 6 0); [0 0 *l*] (0 0 1), (0 0 2), (0 0 3), (0 0 4), (0 0 5), (0 0 6), (0 0 7), (0 0 8), (0 0 9), (0 0 10), (0 0 11); [*h h* 0] (1 1 0), (2 2 0) (3 3 0), (4 4 0) (5 5 0), (6 6 0); [*h* 0 *h*] (2 0 2), (4 0 4), (6 0 6), (8 0 8); [*h h h*] (1 1 1), (2 2 2), (3 3 3) (4 4 4), (5 5 5); [-*h h h*] (-1 1 1), (-2 2 2), (-3 3 3) (-4 4 4), (-5 5 5); and [*h* 0 *h*/2] (2 0 1), (4 0 2), (6 0 3), (8 0 4), (10 0 5). Diffraction-line broadening measurements containing both crystallite domain size and microstrain parameters are given in Table V, while graphic illustrations are shown in Fig. 6.

It can be noticed that the crystallite domain size has different values for both methods. Values for the Warren-Averbach method that is, $<D>_v$ and $<D>_s$, range from 3988 – 10514, and 2192 – 5357Å, respectively. The simplified integral-breadth method $<D_{C-G}>$ has the lowest values ranging from 1766 to 3774 Å. However, the trend is the same for all three measurements, decreasing in following order: [*h* 0 *h*/2]→[*h* 0 *h*]→[*h* 0 0]→[*h h h*]→[0 *k* 0]→[0 0 *l*]→[-*h h h*]→ [*h h* 0].

Similarly to the previous calculations, the microstrain parameters also differ from each other. Values for the Warren-Averbach method are very close ranging from 0.745–

0.986 for RMSM averaged over the $<D>_s$ distance and 0.964 – 0.735 for RMSM averaged over the $<D>_v$ distance. Unlike the crystallite domain size measurements, the highest values for microstrain are of the simplified integral-breadth method $\langle \varepsilon_{C-G} \rangle$ ranging from 0.813 to 1.160. The similar trend, but with different order has been established here: [*h* 0 *h*/2]→[*h* 0 *h*]→[*h* 0 0]→ [0 0 *l*]→[*h h* 0]→[0 *k* 0]→[-*h h h*]→[*h h h*].

Tab. V Crystallite domain size (Å) and microstrain parameters (10^{-3}) obtained by the Warren-Averbach and simplified integral-breadth methods for $La_2SrB_{10}O_{19}$.

	h 0 *h*/2	*h* 0 *h*	*h* 0 0	*h h h*	0 *k* 0	0 0 *l*	*Int.*	-*h h h*	*h h* 0
$<D>_s^{I}$	5257±77	4700±45	4656±23	3917±61	3353±41	3232±26	2866±66	2383±21	2192±23
$<D>_v^{II}$	10514±112	9411±91	9311±46	7834±74	6707±55	6463±64	4521±94	4311±64	3988±36
$<D_{C-G}>^{III}$	3774	3333	3062	2508	2564	2121	2137	1936	1766
$\left\langle \varepsilon^2 \right\rangle^{1/2}_{\langle D_S \rangle/2}$ IV	0.986±0.02	0.961±0.04	0.959±0.02	0.745±0.01	0.776±0.04	0.925±0.05	0.872±0.06	0.754±0.04	0.778±0.02
$\left\langle \varepsilon^2 \right\rangle^{1/2}_{\langle D_V \rangle/2}$ V	0.964±0.03	0.954±0.02	0.952±0.01	0.735±0.03	0.764±0.03	0.915±0.6	0.893±0.04	0.771±0.6	0.797±0.04
$\langle \varepsilon_{C-G} \rangle$ VI	1.160	1.040	0.988	0.813	0.882	0.971	0.937	0.828	0.925

[I]Surface-weighted domain size (Å), [II]Volume-weighted domain size (Å), [III]Volume-averaged domain size from the simplified integral-breadth methods: Cauchy-Gauss function (Å), [IV]Root-mean-square microstrain (RMSM) averaged over the $<D>_s$ distance,[V]RMSM averaged over the $<D>_v$ distance, [VI]Upper limit of microstrain from the simplified integral-breadth methods: Cauchy-Gauss function, Int.-integral sample. (Average bong lengths and BVC were calculated by authors of this study).

4. Conclusion

The structure and microstructure characteristics of $La_2SrB_{10}O_{19}$ were studied in detail. Literature data usually contain one average parameter for crystallite domain size and microstrain measurements per phase/sample [15-20, etc.]. This study consists of microstructure calculations obtained by two methods along with eight crystallographic directions with addition of overall average value. The structure and microstructure characteristics of $La_2SrB_{10}O_{19}$ were studied in detail. The exceptional characteristic of this structure is its novel chemical composition since it is the only isostructural crystal compound with so far known $La_2CaB_{10}O_{19}$. According to the results obtained, substitution of calcium by strontium caused structure disorder. Incorporation of larger Sr instead of Ca into the crystal structure shifted the distance between Sr and La. BVC results revealed that oxygens with the highest (O7) and lowest (O8) values are connected to both La and Sr, thus indicating exact location of disorder. In addition, it is of great importance to emphasize that the highest microstrain values are in the [*h* 0 *h*/2] direction where La – Sr – La cations are situated (Fig. 4b), thus confirming the BVC assumption.

Acknowledgments

Financial support of the Ministry for Education, Science and Technological Development of the Republic of Serbia (Projects No. OI172004 and TR34001) are gratefully acknowledged.

5. References

1. V. G. Dmitirev, G. G. Gurzadyan, D. N. Nikogosyan, Handbook of Nonlinear Optical Crystals, 3rd ed., Springer, New York, 1999.
2. R. Rajaramakrishna, S. Karuthedath, R. V. Anavekar, Journal of Non-Crystalline Solids, 358 (2012) 1667.
3. G. Kaur, O. P. Pandey, K. Singh, Journal of Non-Crystalline Solids, 358 (2012) 2589.
4. Y. Wu, J. Liu, P. Fu, J. Wang, H. Zhou, G. Wang, C. Chen, Chemistry of Materials, 13 (2001) 753.
5. J. Cao, J. Wang, P. Fu, F. Guo, Z. Yang, Y. Wu, Progress of Crystal Growth Characterization, 40 (2000) 97.
6. S. V. Smiljanić, S. R. Grujić, M. B. Tošić, V. D. Živanović, J. N. Stojanović, S. D. Matijašević, J. D. Nikolić, Ceramics International, 40 (1) (2014) 297.
7. S. V. Smiljanić, S. R. Grujić, M. B. Tošić, V. D. Živanović, S. D. Matijašević, J. D. Nikolić, V. S. Topalović, Chemical Industry &Chemical Engineering Quarterly, 22 (1) (2016) 111.
8. S. Smiljanić, E. Karamanova, S. Grujić, J. Rogan, J. Stojanović, S. Matijašević, A. Karamanov, Journal of Non-Crystalline Solids, 481 (2018) 375.
9. H.M. Rietveld, Journal of Applied Crystallography, 2 (1969) 65.
10. J. Rodríguez-Carvajal, Newsletter, 26 (2001) 12.
11. R.G. Garvey, Powder Diffraction, 1 (1986) 114.
12. D. Balzar, H. Ledbetter, Journal of Applied Crystallography, 26 (1993) 97.
13. E. Dowty, ATOMS, Shape Software, Kingsport, Tennessee, USA, 2006.
14. I. D. Brown, Journal of Applied Crystallography, 29 (1996) 479.
15. E-E. C. Osereme, I.B. Iserom, I.E.E Joshua, Science of Sintering, 48 (2016) 221.
16. U. Al-Amani Azlan, A.F.M. Noor, Science of Sintering, 49 (2017) 107.
17. N. Labus, Z. Vasiljević, O. Aleksić, M. Luković, S. Marković, V. Pavlović, S. Mentus, M. V. Nikolić, Science of Sintering, 49 (2017) 455.
18. D. A. Kosanović,V. A. Blagojević, N. J. Labus, N. B. Tadić, V. B. Pavlović, M. M. Ristić, Science of Sintering, 50 (2018) 29.
19. J. Vujančević, A. Bjelajac, J. Ćirković, V. Pavlović, E. Horvath, L. Forró, B. Vlahović, M. Mitrić, Đ. Janaćković, V. Pavlović, Science of Sintering, 50 (2018) 39.
20. M. Mirković, A. Došen, S. Erić, M. Stojmenović, B. Matović, A. Rosić, Science of Sintering, 50 (2018) 95.

Садржај: *Кристална структура новог једињења лантан стронцијум бората утачњена је Ритвелдовом (Rietveld) методом. $La_2SrB_{10}O_{19}$ кристалише моноклинично, просторна група C2 (5), параметри јединичне ћелије a = 11.1170(6), b = 6.5667(3), c = 9.2363(3) Å, β = 91.481°, V = 674.04(7)Å ^{3}, две формулске јединице по ћелији, густина 3.830 g cm^{-3}. Кластери $[B_5O_{12}]$ формирају бесконачне двоструке слојеве који се простиру управно на c-осу. Атоми лантана који су позиционирани у овим слојевима координисани су са десет атома кисеоника у форми LaO_{10} полиедра, док су атоми стронцијума, позиционирани између слојева, координисани са осам атома кисеоника у форми SrO_8 полиедра. Микроструктурна испитивања обухватају мерења величине*

кристалита као и микронапрезања решетке добијена Ворен-Авербаховом (Warren-Averbach) и упрошћеним интегралним методама.
***Кључне речи**: Стакло-керамика, синтеровање, рендгенска дифракција праха, кристална структура и микроструктура, Ритвелдова метода.*